# Towards a Technique for Controlling Wettability Characteristics and Conditioning Film Formation on Polyethylene Terephthalate (PET) Through Laser Surface Engineering

**Waugh, D.G. and Lawrence, J.**



**Original citation:**
Waugh, D.G. and Lawrence, J. (2017) Towards a Technique for Controlling Wettability Characteristics and Conditioning Film Formation on Polyethylene Terephthalate (PET) Through Laser Surface Engineering. Lasers in Engineering, volume 37, issue 4-6, pp. 207-232

Old City Publishing

https://www.oldcitypublishing.com/journals/lie-home/lie-issue-contents/lie-volume-37-number-4-6-2017/lie-37-4-6-p-207-232/

# Towards a Technique for Controlling Wettability Characteristics and Conditioning Film Formation on Polyethylene Terephthalate (PET) Through Laser Surface Engineering

D.G. WAUGH* AND J. LAWRENCE

*School of Mechanical, Aerospace and Automotive Engineering, Faculty of Engineering, Environment and Computing, Coventry University, Gulson Road, Coventry, CV1 2JH, UK*

*Corresponding author: E-mail: david.waugh@coventry.ac.uk

**ABSTRACT**

Bacteria attachment to a surface is initiated by the adsorption of molecules to form a conditioning film (protein layer) on the surface of a substratum. The nature of the substratum strongly influences the composition of the adsorbed protein layer which, in turn, affects the interaction of bacterial cells. Fundamental interactions between proteins adsorbed from bacterial growth media (no-cell adhesion) and $CO_2$ laser surface engineered polyethylene terephthalate (PET). The influence of interfacial wetting on the initial film conditioning of the $CO_2$ laser surface engineered PET was analysed using contact angle measurements, elucidating the relationship between surface roughness parameters, wettability characteristics and conditioning film formation. Chemical analysis of the $CO_2$ laser surface engineered PET surfaces revealed that the recorded changes to the surface energy and wettability were the result of surface morphology changes rather than modification of the chemical structure. The conditioning film adsorbed onto the $CO_2$ laser engineered PET surfaces was found to increase the wetting of the samples. This work demonstrates that $CO_2$ laser irradiation of the surface of PET provides a viable means for controlling interfacial wettability characteristics and conditioning film formation, leading to an effective and efficient means of producing antibacterial surfaces.

*Keywords: $CO_2$ laser, polyethylene terephthalate (PET), conditioning film, biofilm, wettability, contact angle, surface energy, laser surface engineering*

## 1 INTRODUCTION

Preventing bacterial attachment by either anti-biofouling, where bacteria is repelled from the surface, or anti-bactericidal, where the bacteria are inactivated upon coming in to contact with the surface, is a topic of great interest. This because colonisation of bacteria on a surface has, in most cases, an adverse effect on the functionality of the surface (interface) resulting in major health concerns and economic burdens in hospital and industrial environments [1-9]. In the food industry biofilms have been found to persist on food processing equipment, then detach and contaminate other surfaces, including those in direct contact with food, leading to food spoilage problems or potential public health concerns [9-12].

It is widely recognized and accepted that in an aqueous environment bacterial attachment is mediated by the pre-adsorption of proteins to the surface: cells do not attach directly to the substrate surface, rather they attach to proteins adsorbed on to the substrate surface [13-15]. Protein adsorption, commonly called the conditioning film, is a complex process involving non-specific physicochemical mechanisms involving van der Waals, electrostatic interactions and hydrogen bonding [16]. The nature of conditioning films may vary depending on the type of environment the surface is exposed to as proteins adsorb on to surfaces in differing quantities, densities and orientations depending on the chemical and physical characteristics of the surface [16-18]. In addition to this, the protein-surface interactions play an import role in determining the adsorbed conformation, which in turn determines the activity of the surface-bound protein and subsequent cell attachment [19].

Once adsorbed to a surface, conditioning films have been shown to influence the substratum surface properties including surface charge, wettability and surface free energy; all factors involved in influencing the initial attachment of bacteria and subsequent biofilm formation [20, 21]; moreover, it has been suggested that the attachment strength of the initial biofilm is determined by the conditioning film [15] and the final structure and composition of the biofilm is determined by the conditioning film and the extracellular matrix of the biofilm combined [13]. For many pathogens, the interaction between bacterial cells and potential host surface determines the likelihood of the microorganism to colonise and infect the host [22]. Recently, Hsu *et al* [23] found that the size and periodicity of micro- and nanoscale features heavily influences the degree of bacterial attachment to a surface. Attached cells show differences in their size and morphology depending on the topographical features of the surface

Laser modification of polymeric surfaces for the prevention of bacterial attachment could provide a high value adding technique for producing structured surfaces with

superhydrophobic properties that could prevent the attachment of bacteria. Laser surface engineering is a subject of considerable interest at present due to its ability to produce enhanced components with idealized surfaces and bulk properties [24, 25]. Laser surface modification of polymeric materials has been extensively researched over the past decade, resulting in wide application throughout different industries [25-28]. Still, limited research has been focused on the surface modification of polymers for the prevention of bacterial attachment [29].

In this work the surface characteristics and contact angle measurements were investigated in order to explain the relationship between laser modified surface parameters, wettability characteristics and conditioning film formation (the precursor to bacterial attachment) on polyethylene terephthalate (PET) laser surface engineered with a $CO_2$ laser.

## 2 EXPERIMENTAL DETAILS

### 2.1 Material specification and sample preparation procedure

PET films (Goodfellow, Ltd.), biaxially oriented with 0.25 mm thickness were sourced as the experimental substrate. Prior to laser beam exposure the PET films were cleaned in acetone and then in ethanol for three minutes each at room temperature (20$^{o}$C) then dried in a sample drier for a minimum of one hour. Samples were then cut into 10 □ 15 cm$^2$ sheets for experimental convenience.

### 2.2 Laser surface engineering procedure

The surfaces of the PET film samples were laser engineered using a $CO_2$ laser (Firestar; Synrad, Inc.). The $CO_2$ laser emitted a Gaussian beam at 10.60 μm in the continuous wave (CW) mode with a maximum output power of 60 W. The laser beam was delivered to the PET film surface using galvanometric scanning head.

The experimental samples were secured down and positioned at the focal point which was 190.00 mm away from the surface of the sample to the focussing lens on the galvanometric head. All samples were treated in ambient air and an extraction system was used to remove any fumes produced during the $CO_2$ laser processing. The same $CO_2$ laser operating parameters were used for all laser surface engineering configurations: laser power was set to 10% (6 W); transverse speed was set to 400 mm/s; and laser beam diameter was maintained at 95.00 μm.

In order to create the desired pattern upon the PET film sample surfaces Synrad Winmark Pro software was used to scan the $CO_2$ laser beam within a square working field of

110.0 × 110.0 $mm^2$. Two different track and two different hatch patterns were produced - tracks with 350.00 and 400.00 µm spacing between each line were used to produce the different patterns. Track samples were labelled CO2SP_04 and CO2SP_05 and hatch samples were labelled CO2HA_04 and CO2HA_05, for 350.00 and 400.00 µm spacing, respectively, for both patterns. A total of 24 circles with diameters of 15.00 mm were machined of each pattern onto the experimental sample sheets.

### 2.3 Conditioning film growth environment

In order to investigate the effect conditioning film formation had on the wettability of $CO_2$ laser surface engineered and as-received PET film, samples were incubated in different environmental conditions, including tryptone soya broth (TSB), deionised water ($dH_2O$) and ambient (NA) *via* the following procedure.

Previous research by Liu *et al* [30] has found maximum adsorbed protein occurred at an incubation time of approximately one hour and so this time period was adopted for this work. To determine the variation of total protein adsorption onto the PET surfaces samples were incubated with TSB medium and sampled every 10 minutes over a one hour period. After the prescribed time points, the TSB medium was removed from the sample wells samples were gently washed twice in phosphate buffer saline (PBS) to remove any residual medium. After removal of the final wash solution from the cells, 200 µl radioimmunoprecipitation assay (RIPA) buffer was added to the wells and the plate was incubate on ice or in a refrigerator (2 to 8°C) for five minutes. Supernatant was then transferred to a clean sterile microtube then centrifuged at 8000 □g for 10 minutes. Afterwards, the total amount of protein was analysed using Pierce Bironic concentration assay (BCA) (23227; Thermo Scientific, Ltd.).

### 2.4 Physical and chemical surface characterization techniques

Before and after $CO_2$ laser surface engineering the PET sample films were analysed in batches of three each using an optical microscope (DM500; Leica Microsystems, GmbH) and a scanning electron microscope (SEM) (TM3030 Plus; Hitachi Corporation). Surface topography was analysed using a three-dimensional (3-D) profilometer (Micromersure2; STIL SA). Sample sizes of 0.5 □ 0.5 $mm^2$ were examined for each experimental PET film sample. Modified samples were ultrasonically cleaned in acetone, ethanol then $dH_2O$ for three minutes each at room temperature before measurements were taken. The results were analysed using SurfaceMaps (STIL, France) and were expressed as $R_a$ (the arithmetic mean of the departures

of the roughness profile from the mean line) and $S_a$ (the surface roughness calculated over an area) [36]. Data of $R_t$ (maximum height of profile) and $R_{sk}$ (skewness; symmetry of the profile about the mean) surface parameters have also been included in order to provide more information on the topographical features of the surface.

Attenuated total reflectance (ATR) infrared spectroscopy with ZnSe prism and incident angle of 45° was performed using a Fourier transformer – infrared (FTIR) instrument (Scimitar 2000 FTIR; Varian, Inc.) to investigate crystallinity changes of the $CO_2$ laser surface engineered PET. X-ray diffraction (XRD) (D8 Advance; Bruker Corporation) was also used to analyse crystallinity changes.

X-ray photoelectron spectroscopy (XPS) data were acquired using a bespoke ultrahigh vacuum system fitted with a 150.00 mm mean radius hemispherical analyser (Phoibos; Specs, GmbH) with nine-channeltron detection. XPS spectra were acquired using a nonmonochromated Al K X-ray source at 1486.6 eV. Survey spectra were acquired over the binding energy range 1100.0 to 0.0 eV using a pass energy of 50.0 eV and high resolution scans were made over the C 1s and O 1s lines using a pass energy of 15.0 eV. In each case the analysis was an area-average over a region approximately 2.00 mm in diameter on the sample surface. The energy scale of the instrument is calibrated according to ISO standard 15472, and the intensity scale is calibrated using an in-house method traceable to the UK National Physical Laboratory [31]. Data were quantified using Scofield cross-sections corrected for the energy dependencies of the electron attenuation lengths and the instrument transmission. Data interpretation was carried out using CasaXPS software v2.3.16.

### 2.5 Wettability characteristics

Contact angles were measured with a goniometer (OCA20; Dataphysics, GmbH) using the needle-in advancing method. Prior to contact angle measurements being taken, samples were ultrasonically cleaned in ethanol for five minutes each at room temperature (FB 11021; Fisher Scientific, Ltd.). To ensure that the sample surfaces were dry the experimental PET film samples were placed in a specimen dryer (SS; LEEC, Ltd.) for 30 minutes before contact angle measurements were taken. For preconditioned samples, contact angle measurements were taken as described above; however, the samples were not cleaned before analysis. At the prescribed time points each samples was removed and rinsed in $dH_20$ to remove any excess media then allowed to air dry before analysis.

### 2.6 Statistical techniques

Results are reported using mean values and 95% confidence intervals. A two-way analysis of variance (ANOVA) was used to compare groups. Where an interaction relationship was found between the data groups, a simple main mean test was run with pairwise comparisons to find where the statistically significant results were ($p<0.05$). Where no interaction relationship was found the main mean results have been reported, and the pairwise comparisons were made by applying Tukey's Post Hoc analysis. All data has been analysed using IBM SPSS statistics 22 and graphical representation of results were produced using SigmaPlot 13.0.

## 3 RESULTS AND DISCUSSION

### 3.1 Topographical analysis

Optical and SEM micrographs of the $CO_2$ laser engineered surface patterns are given in Figure 1. The optical micrographs of the samples demonstrate the change to the surface of the laser engineered PET samples relative to the as-received control sample. Previous results have shown lasers to be effective tools for engineering specific and unique topographical features upon varying polymeric materials [32-35]. The patterns of the PET film surfaces engineered by the $CO_2$ laser interaction depend upon both the optical system parameters of the laser configuration and the material properties of the polymer [36]. The laser parameters determine the incident laser power, spot size, depth of field and divergence of the laser beam, while the thermophysical properties of the polymer determine how the polymer reacts to the beam. The resulting profile of the engineered patterns and the heat affected zone (HAZ) are a result of the combination of these factors [36]. From the SEM images in Figure 1 one can see that as a direct result of the interaction of the $CO_2$ laser beam with the PET film surface, features were created *via* controlled melting, as evidenced by the craters formed from bubbles and subsequent re-solidification which has formed the different track patterns. This complicated structure is likely associated with the thermally induced stress release in the biaxially oriented film caused by the laser beam interaction with the PET film [37].

In comparison to the track patterns, both hatch patterns have resulted in wider tracks being formed along the ordinate direction of the pattern. This is due to the $CO_2$ laser beam naturally processing the PET surface twice. Initially this occurs in the ordinate then again along the abscissa, and where the laser beam passes over the initial etch track, the PET surface re-melts and solidifies for a second time creating larger surface features. The melting and re-

solidification of the material on the hatch pattern has also resulted in some of the etched patterning being changed. Where the laser beam has passed over the underlying track, the sides have been re-melted and part of the tracks filled in; however the overall hatch and track patterns appear clean and well structured. It is worth noting that no discernible HAZ was observed under optical microscopic analysis, Figure 1, and therefore the areas between the tracks were treated as the as-received material.

The $R_a$ (the arithmetic mean of the departures of the roughness profile from the mean line) parameter was found to have considerably increased from 0.06 ±0.01 µm, up to 8.64 ±0.10 and 6.22 ±0.79 µm for samples CO2SP_04 and CO2SP_05, respectively. The $S_a$ (the surface roughness calculated over an area) parameter was found to have considerably increased from 0.22 ±0.13 µm, up to 22.80 ±4.43 and 10.47 ±0.12 µm for samples CO2SP_04 and CO2SP_05, respectively. The increase in surface roughness between the asreceived samples and both CO2SP_04 and CO2SP_05 samples were found to be statistically significant with a mean difference of 8.58 µm, $p<0.01$, and 6.62 µm, $p<0.01$, for $R_a$ and 22.58 µm, $p<0.01$, and 10.24 µm, $p=0.01$, respectively, for $S_a$ (see Figures 2 to 4).

For samples labelled CO2HA_ both the $R_a$ and $S_a$ surface parameters were found to have increased markedly compared to the as-received sample (see Table 1). The increase in surface roughness between the as-received samples and both hatch patterned samples, CO2HA_04 and CO2HA_05, was found to be statistically significant, $p<0.05$. Interestingly, as well as an overall increase in surface roughness, the surface roughness for sample CO2SP_04 and samples CO2HA_04 were found to significantly increase compared to that of wider spaced track and hatch patterns (_05), $p<0.05$, for both $R_a$ and $S_a$. This is due to a larger surface area of the CO2SP_ 04 and CO2HA_04 samples being processing by the $CO_2$ laser beam, creating a far rougher surface.

The statistical significances between the as-received PET films and the $CO_2$ laser surface engineered is unsurprising as the $CO_2$ laser modification produced well defined topographical features, that can be seen in both the 3-D surface and extracted profiles shown in Figures 2 to 4. The $CO_2$ laser surface engineering of the PET films resulted in an overall increase in surface roughness for all the patterns tested. In comparison to the as-received sample, large topographical features have been created through the laser processing of the tracks. Surfaces with a $R_a$ value of <0.80 µm are typically considered ‘hygienic’, whereas those with a $R_a$ of >0.8 µm more susceptible to bacterial deposition [38]. Having said that, the $R_a$ value does not take into consideration the surface topographical features. This is significant as

these features are well defined and are known to influence the formation of conditioning films and bacterial attachment [23, 38, 39].

The $R_t$ and $R_{sk}$ values given in Table 1 reveal details of the specific surface features of the analysed samples. From Table 1 it can be seen that the hatch patterns overall resulted in surface features that are much larger than that of the single track patterned samples or the asreceived samples. This can be explained, as discussed by the second pass of the $CO_2$ laser beam on the hatch pattern, which was 90.00º to the first pass resulting in double the amount of laser beam interaction on the same spot where the two tracks passed. This can also be seen in the optical and SEM images in Figure 1.

### 3.2 Polymeric microstructural analysis

The complexity of the vibrational spectrum of partially crystalline PET is a result of the spilt of the absorption bands into amorphous and crystalline modes and also the fact that they are sensitive to chain configuration and orientation [40]. Due to this, assignment of the bands to crystalline and amorous regions has proven to be difficult, and led to differences in interpretation; however Chen *et al.* [40] found the carbonyl absorption band has a maximum absorption in the amorphous regions at 1727 and 1717 $cm^{-1}$ in crystalline material, such that on crystallization the intensity of the higher wavenumber band decreases and is progressively shifted to lower wavenumber. These changes, therefore, make the ratio of the two carbonyl absorption bands a convenient method of measuring the fractional crystallinity of PET. Figure 5 compares the ATR-FTIR spectra of the as-received PET film and one representation of the $CO_2$ laser surface engineered PET film. to the spectrum of PET from a database (KnowItAll Informatics System 2014, BioRAD Laboratories). The band at 1717 $cm^{-1}$ has increased from the as-received PET sample to the $CO_2$ laser engineered PET sample, suggesting that $CO_2$ laser engineering of the PET films effected higher crystallinity. The XRD patterns with 2θ between 18.00 and 35.00° of the as-received and $CO_2$ engineered PET films are given in Figure 6. After $CO_2$ laser treatment the peak at 26.00° sharpens and shifts slightly to the left (25.80°) while a peak at 34.20° begins to appear, also suggesting the crystallinity of the PET films has increased after the patterns were engineered on to the surface using the $CO_2$ laser. The $CO_2$ laser-induced re-solidification process favours a more crystalline structure, from which we can infer that the laser process is effectively reducing the level of entanglement within the polymer allowing a somewhat more ordered structure to be established. This is possibly due to the short, but intense, melt applied by the laser as infrared wavelengths act as heat sources. The abrupt, and

directional, removal of the heat source caused by the rapid processing may be what facilitates this ordering of the polymer.

### 3.3 Chemical analysis

XPS was used to investigate any changes in surface chemistry of the PET film samples. Results of the quantitative surface analyses of the as-received and four $CO_2$ laser surface engineered PET samples are given in Table 3. In all cases the data show C and $O_2$ in approximately the corrected atomic ratio expected for a pure PET reference sample, along with a number of lower level species. The lower level species include N, Ca, Na, S, P, Si and F. These are typical surface contamination elements resulting from handling, and general exposure to the laboratory environment, and the amounts detected indicate sub-monolayer levels on the outer surface of the samples. The overall level of these surface contaminant species was reduced by the laser treatments, possibly as a result of local surface vaporisation as a consequence of the input laser energy.

Spectra from all samples were very similar. The survey spectrum and the higher resolution scans over the C 1s and O 1s lines from the CO2_SP04 sample are shown in Figure 7. Apart from the presence of the minor surface contaminant species, the spectra are in very good agreement with reference data from pure spin-cast PET [41]. The C 1s spectrum shows components due to carbon-carbon bonds, carbon in ether bonds and carbon in ester bonds, and the O 1s spectrum shows components due to oxygen in ether and carbonyl/ester groups as expected. There was no significant modification of the number or relative proportions of these components through the series of samples investigated. In summary, the data show no change in surface chemistry of the PET surfaces after laser treatment, apart from small differences in the levels of trace contaminants. This demonstrates that the laser process is capable of generating surface features without modifying the chemical composition of the layer. This is important as it reveals that the changes to the surface energy and wettability of the PET, as discussed above, are due entirely to surface morphology changes rather than modification of the chemical structure, which would undesirably change its innate properties.

### 3.4 Conditioning film analysis

3.4.1 Findings in terms of wettability

The wetting phenomena has been widely studied both theoretically and experimentally in connection with the physics of surfaces and interfaces [42-46] and it has previously been suggested that water contact angle measurements could be used as an indicator of microbial colonisation on a surface [47]. It has been found that intermediate contact angles of 30.00 to 100.00$^{o}$ do not possess features that are described as 'easy clean', meaning that the removal of bacterial and other contaminants is particularly hard, and the raised features provide platforms that are easier for microbes to adhere to, and subsequently form a biofilm [48]. It can, therefore, be argued that surfaces which are either superhydrophilic ($\leq$10.00$^{o}$) or superhydrophobic ($\geq$150.00$^{o}$) are more likely to prevent the attachment of bacteria. Our findings show that the $CO_2$ laser was highly effective in increasing the surface hydrophobicity of the PET surfaces ($p<0.05$). For the track patterns, $CO_2$ laser surface engineering resulted in an increase in the surface contact angles by almost 100% over asreceived contact angle measurements. This implies that the $CO_2$ laser has modified the PET film surface to such a degree that hydrophobic surfaces for all patterns tested in this study are greater than 100.00$^{o}$. According to Fadeeva *et al* [32], contact angles greater than 100.00$^{o}$ might be sufficient in preventing bacteria from adhering to surfaces and so our $CO_2$ laser surface engineered surfaces may be effective as they are in preventing the formation of biofilms. Wetting of solid surfaces, as can be seen from the results presented herein, is sensitive to surface geometrical changes induced by the $CO_2$ laser surface modification. This initial change in contact angle measurement of the laser modified surface suggests that the surface would be harder for microbes to colonise in comparison to the as-received PET film (see Table 2).

As a conditioning film forms the wettability of the surface changes. The change in contact angle has been measured over time with conditioning films forming in the presence of no media and two different incubation medium, deionised water (dH2O) and TSB. The contact angle measurements showed wettability properties decreased significantly from 137.40 to 115.60$^{o}$ and 143.20 to 110.80$^{o}$ for CO2SP_04 and CO2SP_05, respectively, within the first 10 minutes of being submerged in the TSB media. This difference remain constant for the rest of the incubation period, as one can see from Figure 8. The conditioning film formation deposited on the CO2HA_04 and CO2HA_05 increases the wettability of the hatched material considerably after 60 minutes for both CO2HA_04 and CO2HA_05 (see Figure 9). For CO2HA_05 specifically, at this time point, the wettability difference between the pattern and

the as-received samples appears to be removed; however, this difference was still determined to be statistically significant, p=0.04. It is possible here that due to the larger surface features created by the $CO_2$ laser, there was a larger surface area available for the protein in the conditioning film and this consequently increased the rate at which proteins can adsorb on to the surface, resulting in the conditioning film forming quicker when compared to the track patterned samples. As previously discussed by Taylor *et al* [21], the conditioning film has been found to influence substratum surface properties including surface charge, wettability and surface free energy, which have been shown to be factors influencing the initial attachment of bacteria and subsequent biofilm formation. In this work we can state that the formation of the protenious film is heavily influenced by the topographical features of the substratum. This is highlighted by the difference in wettability characteristics between the trench *versus* the hatch and as-received PET sample post-conditioning film formation; indeed, it can be argued that the formed protenious film has a stronger influence on the wettability characteristics than that of the topographical features.

The TSB conditioning film is responsible for reducing the hydrophobic characteristics of the $CO_2$ laser surface engineered PET films. The large error bars of the TSB samples can be explained by a nonhomogeneous layer of proteins and macromolecules adsorbing on to the surface which has previously been shown by Lee *et al* [20] to be influenced by different surface features. No correlation was found between samples incubated in absence of media (NA) or deionised water (H20) and changes in the wettability characteristics.

### 3.4.2 Findings in terms of surface energy

Surface energy has been previously reported to be of great importance in the biofouling of surfaces [49, 50]. The surface energy of a solid surface provides a direct measurement of the intermolecular or interfacial attractive forces. The influence of surface energy of modified surfaces on bacterial adhesion has had conflicting reports highlighting the complex nature of the interaction of difference bacterial species with surfaces with different ranging surface energies [49-51]. Liu *et al* [49] concluded that bacterial adhesion may decrease or increase with increasing surface energy of substrates, depending on the physical and chemical properties of the bacteria, substrates and aqueous environment. In the work presented herein the surface energy of all the patterns tested increased following submersion in the TSB medium, as can be seen from Figure 10 and Figure 11. It is possible to predict that this increase in surface energy would most likely result in an increase in bacterial attachment; however, initially the surface

energy of the modified samples was statistically significantly greater than that of the as-received sample, suggesting that the laser induced patterns present here would initially reduce the likelihood of bacterial adhesion during the first 50 minutes of submersion into the TSB media.

### 3.4.3 Findings in terms of protein adsoption

Understanding the mechanisms of protein adsorption onto surfaces which have been topographically changed could provide an insight in to how surface topography affects protein adsorption and the resultant impact this may have to the biofouling of surfaces. Biological milieu, such as blood and culture media are examples of multi-component solutions and their competitive adsorption, denaturation on the surface, and blood clotting are directly involved with overall biocompatibility and performance [52].

Figure 12 shows the variation of the total amount of protein adsorbed on the sample surface of the different patterned samples in TSB medium, as a function of incubation time. The maximum adsorbed proteins occurred at an incubation time of 30 minutes for the asreceived (CO2_AR) sample, after this the adsorbed mass decreases. Interestingly, the $CO_2$ laser surface engineered samples show that all etched patterns caused a similar pattern for protein adsorption for all of the changed surfaces which were different to that of the asreceived patterns. The initial increase in the quantity of protein adsorbed on to the surface, this could be explained by the increase in surface roughness which has created a larger surface area for the proteins to adhere to. The various changes in protein adsorption on to the different surfaces can be explained due to the competitive protein exchange on the surface, known as the Vroman effect [30]. In general, the Vroman effect has proteins adsorbing from mixtures through a series of adsorption-displacement steps in which already adsorbed proteins are displaced by proteins arriving with a higher affinity [30, 53]. This change in protein adsorption is very much time dependant. It is possible to conclude that the protein adsorption on to the laser modified surfaces affected the total protein adsorption, and thus that the changes in surface structure caused by the laser resulted in different proteins having a higher affinity to the modified surfaces. Having said that, further analysis of how the protein adsorption is affected is required including chemical analysis in order to determine if this is the case.

## 4 CONCLUSIONS

$CO_2$ laser engineering created defined tracks on the surface of the polyethylene terephthalate (PET) films accompanied by changes in the crystalline structure and overall increase in surface roughness and subsequent changes to the wettability characteristics. $CO_2$ laser surface engineering of PET increased the hydrophobicity of the PET samples. Each laser engineered pattern showed an increase in contact angle from 77.70° to angles equalling or greater than 110.00°. Chemical analysis showed no significant change in surface chemistry as a result of $CO_2$ laser treatment; therefore, the increased hydrophobicity is attributed to physical changes in the surface texture and morphology. The trench patterns demonstrated a larger increase in contact angle, up to 143.00°. Within the first 10 minutes of being submerged in a tryptone soya broth (TSB) media the contact angle decreased from 137.40 to 115.60$^o$ and 143.20 to 110.80$^o$ for samples CO2SP_04 and CO2SP_05, respectively. This difference remained constant for the rest of the incubation period. The TSB conditioning film formation deposited on the CO2HA_04 and CO2HA_05 samples was found to increases the contact angle of the hatched patterned PET. Although the TSB conditioning film reduced the overall hydrophobic characteristics of the laser processed surfaces, the track patterns were shown to be the most promising surface design for preventing bacterial attachment as the surface remained hydrophobic ($\theta$>100°). This work provides an inroad into the development of a $CO_2$ laser surface engineering technique for controlling wettability and conditioning film formation, ;leading to the prevention of bacterial attachment.

## REFERENCES


[1] Donlan R.M. Biofilms: Microbial life on surfaces. *Emerging Infectious Diseases* **8**(9) (2002), 881-890.

[2] Reysenbach A.L. and Cady S.L. Microbiology of ancient and modern hydrothermal systems. *Trends Microbiology* **9**(2) (2001), 79-86.

[3] Stoodley P., Sauer K., Davies D.G. and Costerton J.W. Biofilms as complex differentiated communities. *Annual Review Microbiology* **56** (2002), 187-209.

[4] Hall-Stoodley L., Costerton J.W. and Stoodley P. Bacterial biofilms: From the natural environment to infectious diseases. *Nature Reviews Microbiology* **2** (2004), 95-108.

[5] Lewis K. Persister cells, dormancy and infectious disease. *Nature Reviews Microbiology* **5** (2007), 48-56.

[6] Bryers J.D. Medical biofilms. *Biotechnology and Bioengineering* **100**(1) (2008), 1-18.

[7] Gubner R. and Beech I.B. The effect of extracellular polymeric substances on the attachment of Pseudomonas NCIMB 2021 to AISI 304 and 316 stainless steel. *Biofouling* **15**(1-3) (2000), 25-36.

[8] Scheuerman T.R., Camper A.K. and Hamilton M.A. Effects of substratum topography on bacterial adhesion. *Journal of Colloid and Interface Science* **208**(1) (1998), 23-33.

[9] Robitaille G., Choiniere S., Ells T. Deschenes L. and Mafu A.A. Attachment of Listeria innocua to polystyrene: Effects of ionic strength and conditioning films from culture media and milk proteins. *Journal of Food Protection* **77**(3) (2014), 427-434.

[10] Midelet G. and Carpentier B. Transfer of microorganisms, including Listeria monocytogenes, from various materials to beef. *Applied and Environmental Microbiology* **68**(8) (2002), 4015-4024.

[11] Marchand S., De Block J., De Jonghe V., Coorevits A., Heyndrickx M. and Herman L. Biofilm formation in milk production and processing environments: Influence on milk quality and safety. *Comprehensive Reviews in Food Science and Food Safety* **11**(2) (2012), 133-147.

[12] Flint S.H.H., Brooks J.D.D. and Bremer P.J.J. Biofilms in dairy manufacturing plantdescription, current concerns and methods of control. *Biofouling: The Journal of Bioadhesion and Biofilm Research* **11**(1) (1997), 81-97.

[13] Boland T., Latour R. and Stutzenberger F. Molecular basis of bacterial adhesion. in An Y. and Friedman R. (Eds.) *Handbook of Bacterial Adhesion*. New York: Humana Press. 2000. pp. 29-41.

[14] Siboni N., Lidor M., Kramarsky-Winter E. and Kushmaro A. Conditioning film and initial biofilm formation on ceramics tiles in the marine environment. *FEMS Microbiology Letters* **274**(1) (2007), 24-29.

[15] Busscher H.J. and van der Mei H.C. Physico-chemical interactions in initial microbial adhesion and relevance for biofilm formation. *Advances in Dental Research* **11**(1) (1997), 24-32.

[16] Roach P., Farrar D. and Perry C.C. Interpretation of protein adsorption: Surfaceinduced conformational changes. *Journal of the American Chemical Society* **127**(22) (2005), 8168-8173.

[17] Lorite G.S., Rodrigues C.M., de Souza A.A., Kranz C., Mizaikoff B. and Cotta M.A. The role of conditioning film formation and surface chemical changes on Xylella fastidiosa adhesion and biofilm evolution. *Journal of Colloid and Interface Science* **359**(1) (2011), 289-295.

[18] Hao L. and Lawrence J. On the role of $CO_2$ laser treatment in the human serum albumin and human plasma fibronectin adsorption on zirconia (MGO-PSZ) bioceramic surface. *Journal of Biomedical Materials Research, Part A* **69**(4) (2004), 748-756.

[19] Roach P., Farrar D. and Perry C.C. Surface tailoring for controlled protein adsorption: Effect of topography at the nanometer scale and chemistry. *Journal of the American Chemical Society* **128**(12) (2006), 3939-3945.

[20] Lee M., Zheng D., Sharma S.K., Troy P.J., Gyananath G. and Taylor G.T. Influence of surface properties on accumulation of conditioning films and marine bacteria on substrata exposed to oligotrophic waters. *Biofouling* **11**(1) (1997), 31-57.

[21] Taylor R.K., Pomianek M.E., Semmelhack M.F., Kraml C.M., Higgins D.A. and Bassler B.L. The major: Vibrio cholerae autoinducer and its role in virulence factor production. *Nature* **450** (2007), 883-886.

[22] Christensen G.D., Simpson W.A., Younger J.J., Baddour L.M., Barrett F.F., Melton D.M. and Beachey E.H. Adherence of coagulase-negative staphylococci to plastic tissue culture plates: A quantitative model for the adherence of staphylococci to medical devices. *Journal of Clinical Microbiology* **22**(6) (1985), 996-1006.

[23] Hsu L.C., Fang J., Borca-Tasciuc D.A., Worobo R.W. and Moraru C.I. Effect of micro- and nanoscale topography on the adhesion of bacterial cells to solid surfaces. *Applied and Environmental Microbiology* **79**(8) (2013), 2703-2712.

[24] Steen W.M. *Laser Material Processing*. New York: Springer. 2003.

[25] Waugh D.G. and Lawrence J. Laser surface processing of polymers for biomedical application. in Dutta Majumdar J. and Manna I. (Eds.) *Laser Assisted Fabrication of Materials*. Berlin: Springer. 2012.

[26] Ozdemir M. and Sadikoglu H. A new and emerging technology: Laser-induced surface modification of polymers. *Trends in Food Science & Technology* **9**(4) (1998), 159-167.

[27] Zhang Y., Lowe R., Harvey E., Hannaford P. and Endo A. High aspect-ratio micromachining of polymers with an ultrafast laser. *Applied Surface Science* **186**(1-4) (2002), 345-351.

[28] Pfleging W., Bruns M., Welle A. and Wilson S. Laser-assisted modification of polystyrene surfaces for cell culture applications. *Applied Surface Science* **253**(23) (2007), 9177-9184.

[29] Poleunis C., Rubio C., Compère C. and Bertrand P. ToF–SIMS chemical mapping study of protein adsorption onto stainless steel surfaces immersed in saline aqueous solutions. *Applied Surface Science* **203-204** (2003), 693-697.

[30] Liu L., Ercan B., Sun L., Ziemer K.S. and Webster T.J. Understanding the role of polymer surface nanoscale topography on inhibiting bacteria adhesion and growth. *ACS Biomaterials Science & Engineering* **2**(1) (2016), 122-130.

[31] Seah M.P. and Spencer S.J. Repeatable intensity calibration of an X-ray photoelectron spectrometer. *Journal of Electron Spectroscopy and Related Phenomena* **151**(3) (2006), 178-181.

[32] Fadeeva E., Truong V.K., Stiesch M., Chichkov B.N., Crawford R.J., Wang J. and Ivanova E.P. Bacterial retention on superhydrophobic titanium surfaces fabricated by femtosecond laser ablation. *Langmuir* **27**(6) (2011), 3012-3019.

[33] Korte F., Serbin J., Koch J., Egbert A., Fallnich C., Ostendorf A. and Chichkov B.N. Towards nanostructuring with femtosecond laser pulses. *Applied Physics A: Materials Science & Processing* **77**(2) (2003), 229-235.

[34] Kurella A. and Dahotre N.B. Review paper: Surface modification for bioimplants: The role of laser surface engineering. *Journal of Biomaterials Applications* **20**(1) (2005), 5-50.

[35] Gillett A., Waugh D.G., Lawrence J., Swainson M. and Dixon R. Laser surface modification for the prevention of biofouling by infection causing Escherichia Coli. *Journal of Laser Applications* **28**(2) (2016), 022503.

[36] Snakenborg D., Klank H. and Kutter J.P. Microstructure fabrication with a $CO_2$ laser system. *Journal of Micromechanics and Microengineering* **14**(2) (2003), 182-191.

[37] Dyer P.E., Oldershaw G.A. and Sidhu J. $CO_2$ laser ablative etching of polyethylene terephthalate. *Applied Physics B: Lasers and Optics* **48**(6) (1988), 489-493.

[38] Flint B.J., Brooks J.D. and Bremer P.J. Properties of the stainless steel substrate, influencing the adhesion of thermo-resistant streptococci. *Journal of Food Engineering* **43**(4) (2000), 235-242.

[39] Anselme K., Davidson P., Popa A.M., Giazzon M., Liley M. and Ploux L. The interaction of cells and bacteria with surfaces structured at the nanometre scale. *Acta Biomaterialia* **6**(10) (2010), 3824-3846.

[40] Chen Z., Hay J.N. and Jenkins M.J. FTIR spectroscopic analysis of poly(ethylene terephthalate) on crystallization. *European Polymer Journal* **48**(9) (2012), 1586-1610.

[41] Beamson G.B. and Briggs D. High resolution XPS of organic polymers: The Scienta ESCA300 database. *Journal of Chemical Education* **70**(1) (1993), 25-30.

[42] Chow T.S. Wetting of rough surfaces. *Journal of Physics: Condensed Matter* **10**(27) (1998), 445-451.

[43] Agathopoulos S. and Nikolopoulos P. Wettability and interfacial interactions in bioceramic-body-liquid systems. *Journal of Biomedical Materials Research* **29**(4) (1995) 421-429.

[44] Cassie A. and Baxter S. Wettability of porous surfaces. *Transactions of the Faraday Society* **40** (1944), 546-551.

[45] Eginton P.J., Gibson H., Holah J., Handley P.S. and Gilbert P. The influence of substratum properties on the attachment of bacterial cells. *Colliods and Surfaces B: Biointerfaces* **5**(3-4) (1995), 153-159.

[46] Waugh D.G and Lawrence J. Wettability and osteoblast cell response modulation through UV laser processing of nylon 6, 6. *Applied Surface Science* **257**(21) (2011), 8798-8812.

[47] Armentano I., Arciola C.R., Fortunati E., Ferrari D., Mattioli S., Amoroso C.F., Rizzo J., Kenny J.M., Imbriani M. and Visai L. The interaction of bacteria with engineered nanostructured polymeric materials: A review. *The Scientific World Journal* 2014 (2014), 410423.

[48] Page K., Wilson M. and Parkin I.P. Antimicrobial surfaces and their potential in reducing the role of the inanimate environment in the incidence of hospital-acquired infections. *Journal of Materials Chemistry* **19** (2009), 3819-3831.

[49] Liu Y. and Zhao Q. Influence of surface energy of modified surfaces on bacterial adhesion. *Biophysical Chemistry* **117**(1) (2005), 39-45.

[50] Bakker D.P., Huijs F.M., de Vries J., Klijnstra J.W., Busscher H.J. and van der Mei H.C. Bacterial deposition to fluoridated and non-fluoridated polyurethane coatings with different elastic modulus and surface tension in a parallel plate and a stagnation point flow chamber. *Colloids and Surfaces B: Biointerfaces* **32**(3) (2003), 179-190.

[51] Pereni C.I., Zhao Q., Liu Y. and Abel E. Surface free energy effect on bacterial retention. *Colloids and Surfaces B: Biointerfaces* **48**(2) (2006), 143-147.

[52] Kim J-H. and Yoon J-Y. Protein adsorption on polymer particles. in Hubber A.T. (Ed.) *Encyclopedia of Surface and Colloid Science*. New York: Marcel Dekker. 2002.

[53] Noh H. and Vogler E.A. Volumetric interpretation of protein adsorption: Competition from mixtures and the Vroman effect. *Biomaterials* **28**(3) (2007), 405-422.

TABLE 1

Surface parameter data for the PET experimental samples.

| **Sample Pattern** | $R_a$ **(µm)** | $S_a$ **(µm)** | $R_t$ **(µm)** | $R_{sk}$ |
|---|---|---|---|---|
| CO2_AR | 0.06 ±0.01 | 0.22 ±0.13 | 0.36 ±0.04 | -0.09 ±0.24 |
| CO2SP_04 | 8.58 ±0.91 | 22.8 ±4.43 | 49.03 ±8.43 | 0.45 ±0.41 |

| | | | | |
|---|---|---|---|---|
| CO2SP_05 | 6.22 ±0.79 | 10.47 ±0.12 | 43.50 ±5.05 | 0.06 ±0.26 |
| CO2HA_04 | 16.13 ±1.33 | 35.23 ±3.12 | 107 ±2.65 | -1.21 ±0.47 |
| CO2HA_05 | 13.07 ±0.81 | 22.8 ±0.92 | 116 ±4.36 | -0.98 ±0.77 |

TABLE 2

Contact angle measurements formed by water droplets on the $CO_2$ laser engineered PET samples and the corresponding surface energy values.

| **Sample Pattern** | **Contact Angle Measurement, θ (°)** | **Surface Energy, γ ($mJ/m^2$) $_{sv}$** |
|---|---|---|
| CO2_AR | 77.73 ±2.23 | 36.51 ±0.42 |
| CO2SP_04 | 137.41 ±2.30 | 4.25 ±2.29 |
| CO2SP_05 | 143.20 ±2.85 | 2.52 ±0.71 |
| CO2HA_04 | 114.23 ±4.42 | 15.28 ±0.91 |
| CO2HA_05 | 116.19 ±5.48 | 17.58 ±5.64 |

TABLE 3

Surface compositions of the as-received and $CO_2$ laser engineered PET samples as determined by XPS. Normalised to 100% excluding H and He, which are not detected by the technique.

| Element and Photoelectron Line | ce Compositi (at .%) | | | | |
|---|---|---|---|---|---|
| | CO2_AR | CO2SP_04 | CO2SP_05 | CO2HA_04 | CO2HA_05 |
| Na 1s | 0.3 | | | | |
| O 1s | 24.6 | 26.6 | 26.2 | 26.0 | 26.1 |
| N 1s | 2.2 | 0.7 | 0.4 | 1.1 | 0.6 |
| Ca 2p | 0.3 | | | | |
| C 1s | 71.7 | 72.5 | 73.0 | 71.7 | 72.6 |
| S 2p | 0.2 | | | | |
| P 2p | 0.1 | | | | |
| Mg 2s | 0.7 | 0.2 | 0.3 | 0.4 | 0.4 |
| Si 2s/2p | 0.03 | | 0.1 | 0.7 | 0.2 |
| F 1s | | | | | 0.2 |

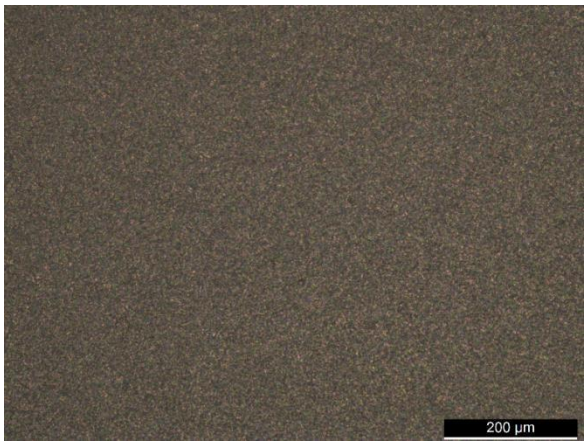


(a)

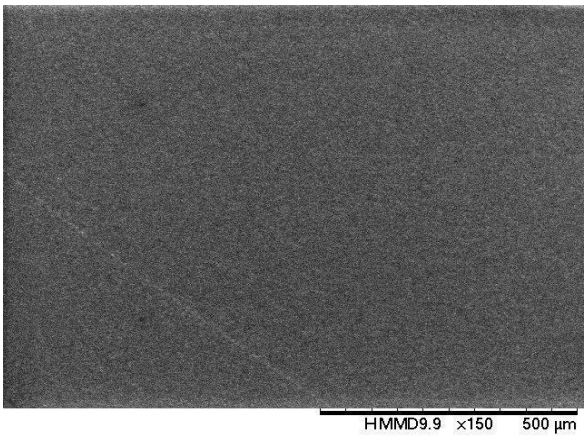


(b)

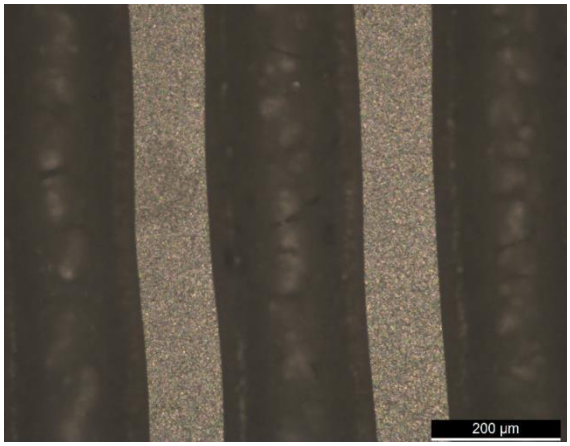
200 µm

(c)

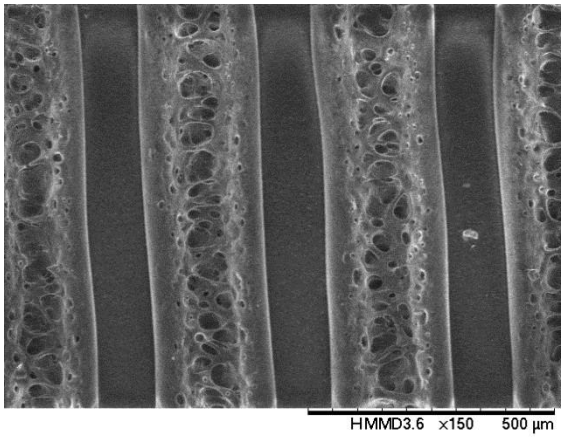
HMMD3.6 x150 500 µm

(d)

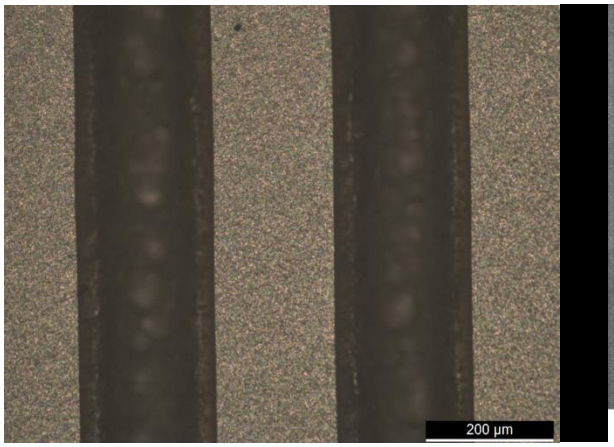
200 µm

(e)

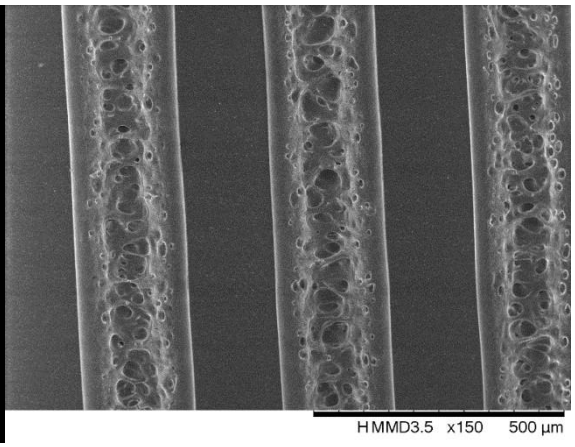
HMMD3.5 x150 500 µm

(f)

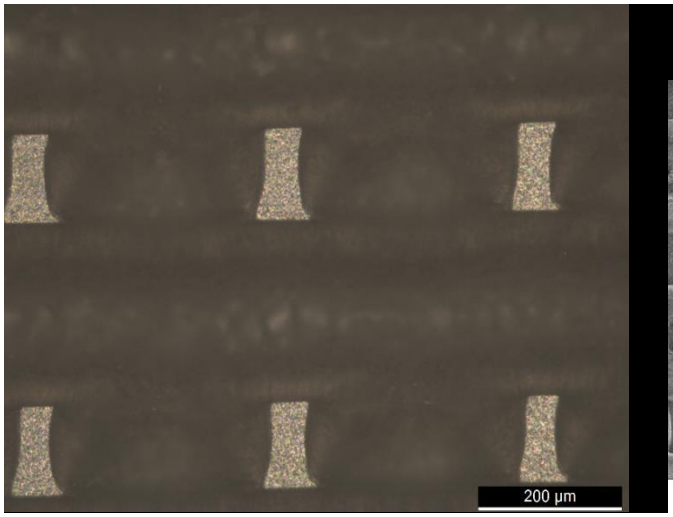
200 µm

(g)

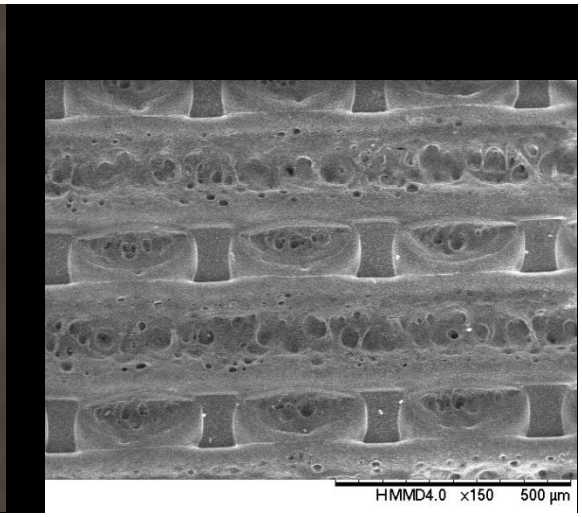
HMMD4.0 x150 500 µm

(h)

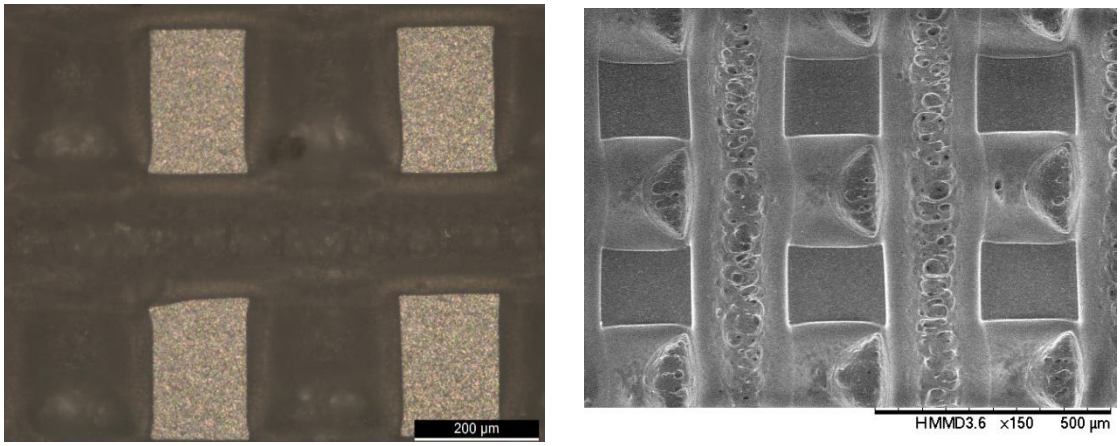


(i) (j)

FIGURE 1

Optical and SEM micrographs of as-received and $CO_2$ laser surface engineered PET films: (a and b) CO2SP_AR; (c and d) CO2SP_04; (e and f) CO2SP_05; (g and h) CO2HA_04; and (I and j) CO2HA_05.

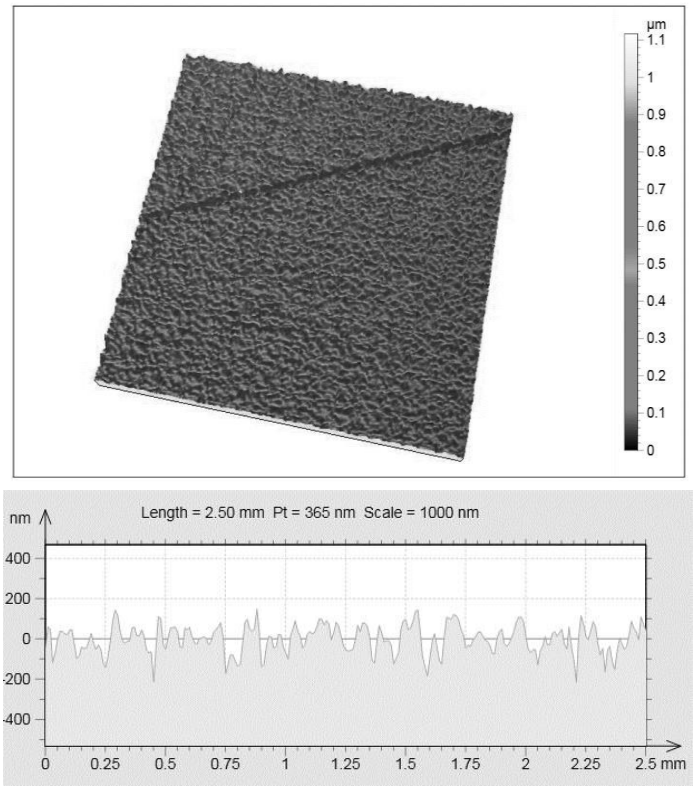


FIGURE 2

3-D surface profile (upper) and profile extraction (lower) for the as-received PET sample (CO2_AR).

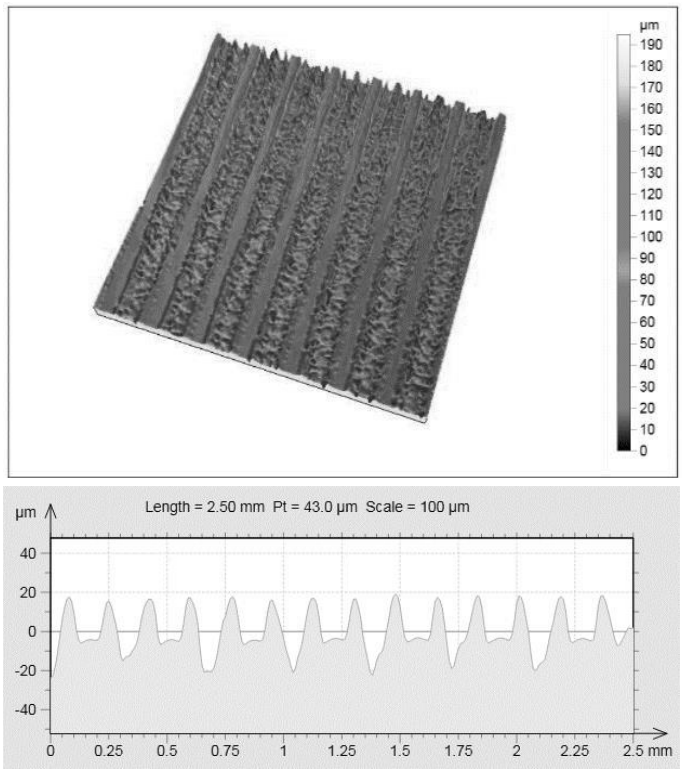
µm
190
180
170
160
150
140
130
120
110
100
90
80
70
60
50
40
30
20
10
0
Length = 2.50 mm Pt = 43.0 µm Scale = 100 µm
µm
40
20
0
-20
-40
0
0.25
0.5
0.75
1
1.25
1.5
1.75
2
2.25
2.5 mm

(a)

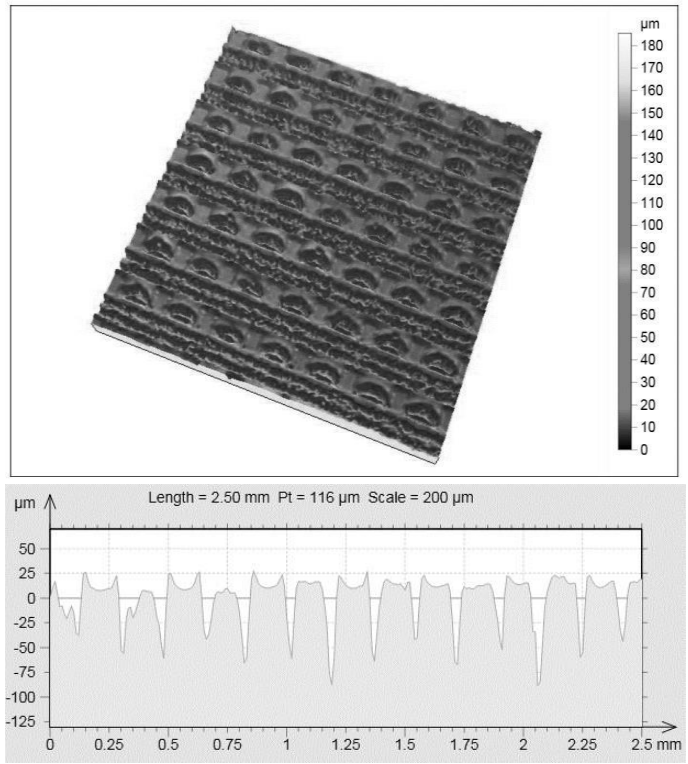
µm
180
170
160
150
140
130
120
110
100
90
80
70
60
50
40
30
20
10
0
Length = 2.50 mm Pt = 116 µm Scale = 200 µm
µm
50
25
0
-25
-50
-75
-100
-125
0
0.25
0.5
0.75
1
1.25
1.5
1.75
2
2.25
2.5 mm

(b)

FIGURE 3

3-D surface profile (upper) and profile extraction (lower) for $CO_2$ laser surface engineered PET samples for 350.00 µm (a) track pattern (CO2SP_04) and (b) hatch pattern (CO2HA_04).

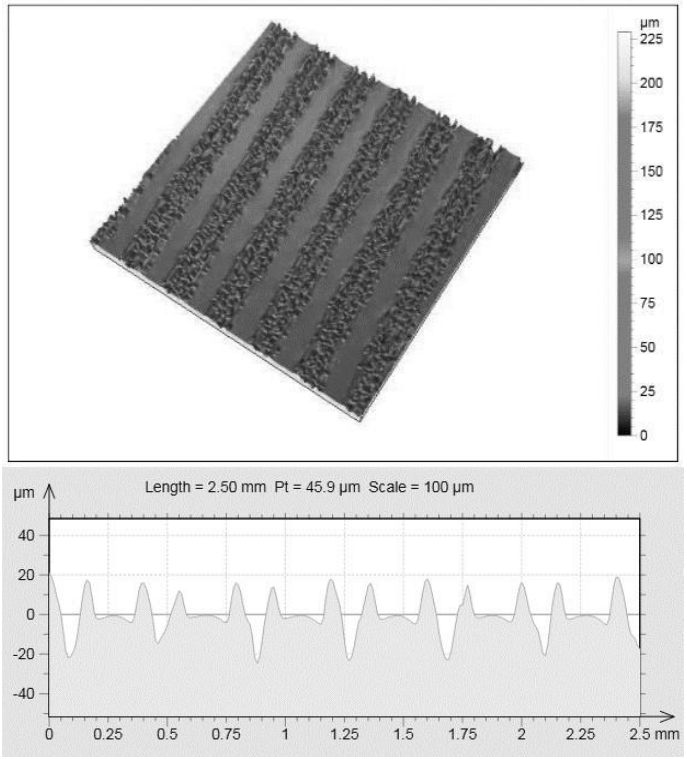
µm
225
200
175
150
125
100
75
50
25
0
Length = 2.50 mm Pt = 45.9 µm Scale = 100 µm
µm
40
20
0
-20
-40
0
0.25
0.5
0.75
1
1.25
1.5
1.75
2
2.25
2.5 mm

(a)

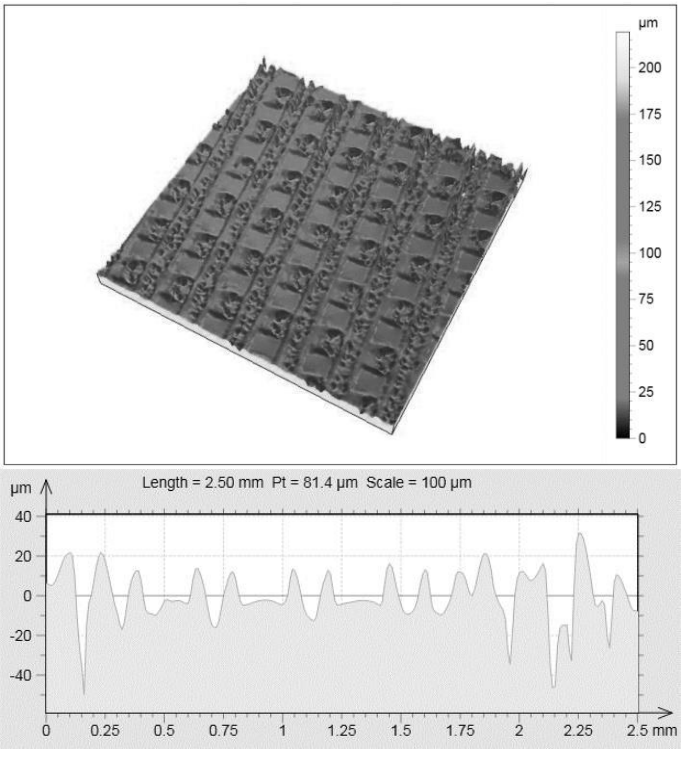
µm
200
175
150
125
100
75
50
25
0
Length = 2.50 mm Pt = 81.4 µm Scale = 100 µm
µm
40
20
0
-20
-40
0
0.25
0.5
0.75
1
1.25
1.5
1.75
2
2.25
2.5 mm

(b)

FIGURE 4

3-D surface profile (upper) and profile extraction (lower) for $CO_2$ laser surface engineered PET samples for 400.00 µm (a) track pattern (CO2SP_05) and (b) hatch pattern (CO2HA_05).

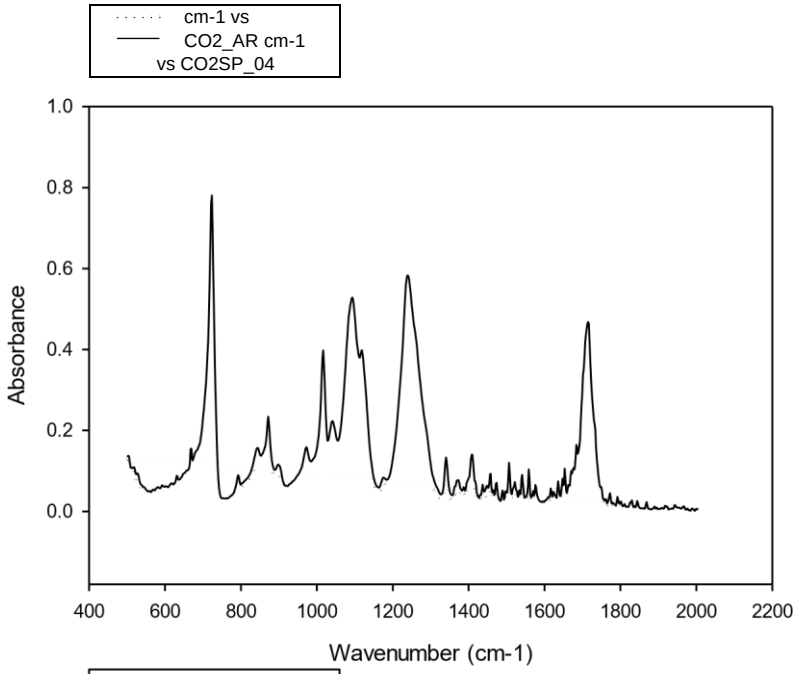


FIGURE 5 ATR-FTIR spectrum of the as-received PET sample (CO2_AR) and $CO_2$ laser surface engineered PET sample with 350 µm track spacing of (CO2SP_04).

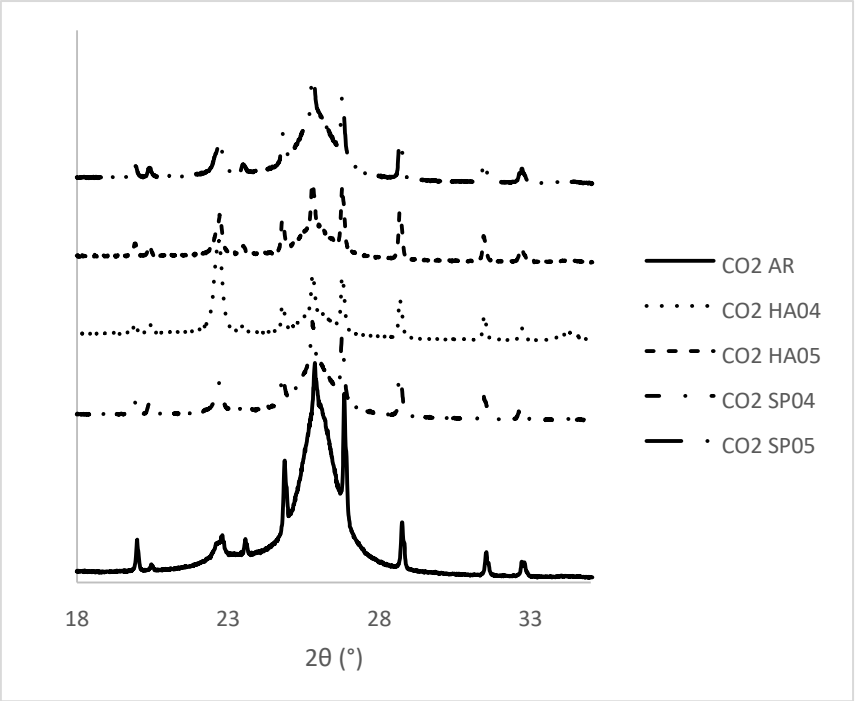


FIGURE 6

XRD spectra of the as-received and $CO_2$ laser surface engineered PET films.

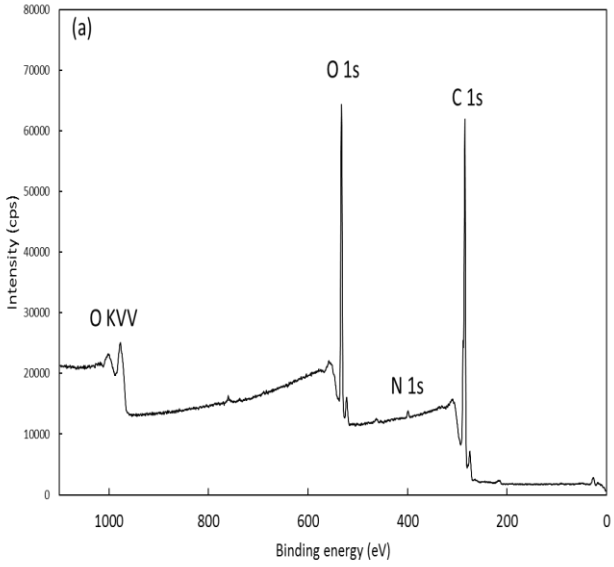
(a)
O 1s
C 1s
O KVV
N 1s
Intensity (cps)
Binding energy (eV)
80000
70000
60000
50000
40000
30000
20000
10000
0
1000
800
600
400
200
0

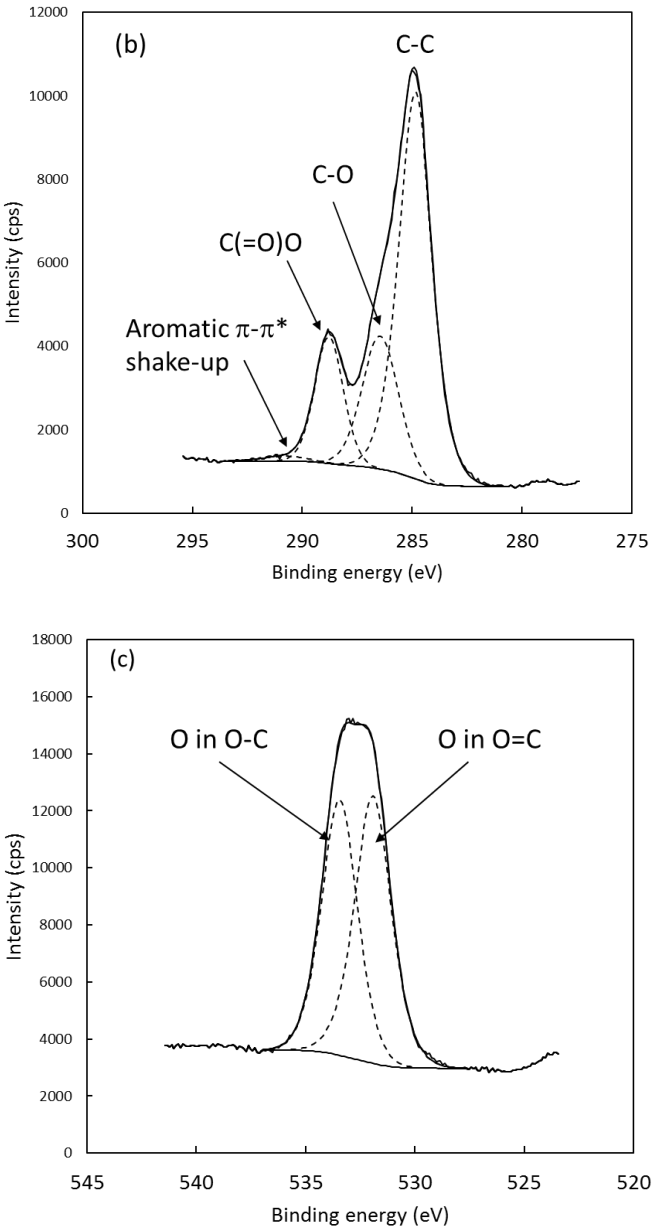


FIGURE 7

XPS spectra from the surface of sample CO2SP_04 showing (a) survey spectrum with principal peaks labelled (the small peak at around 760 eV binding energy is an artefact and should be ignored), (b) and (c) higher resolution C 1s and O 1s spectra with chemicallyshifted components labelled.

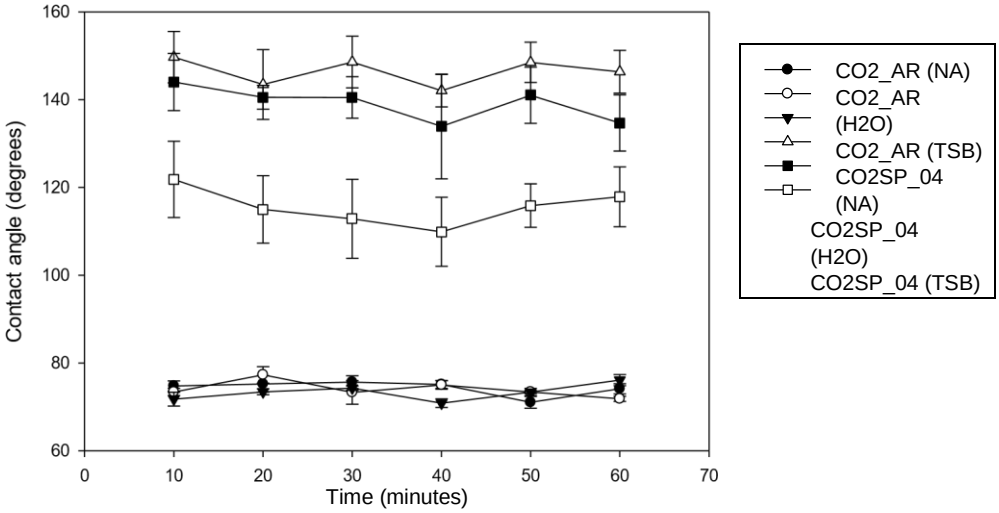


(a)

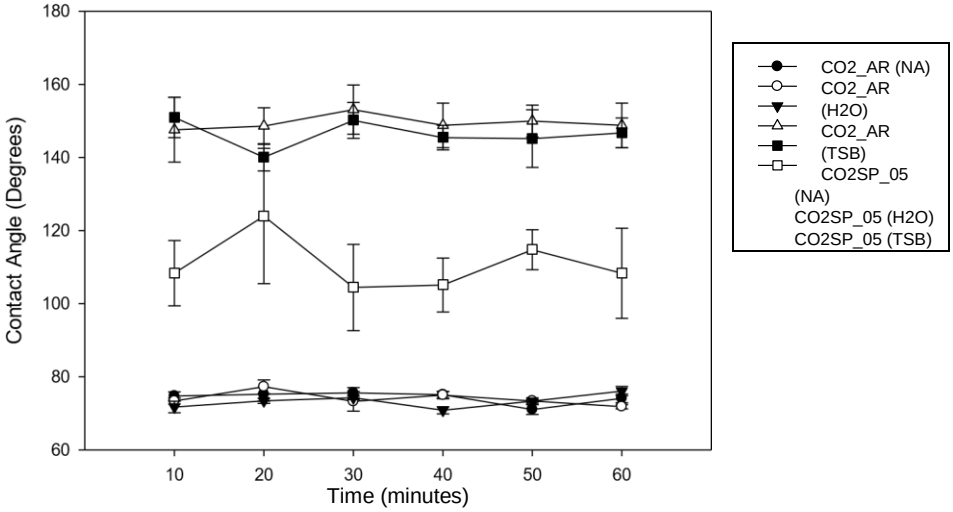


(b)

FIGURE 8

Comparison contact angle measurements of (a) CO2SP_04 with CO2_AR and (b) CO2SP_05 with CO2_AR.

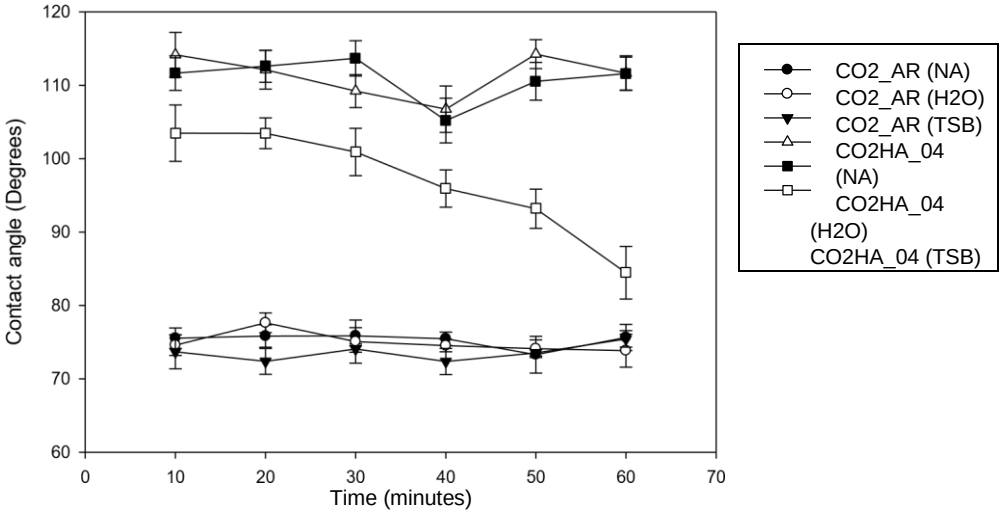


(a)

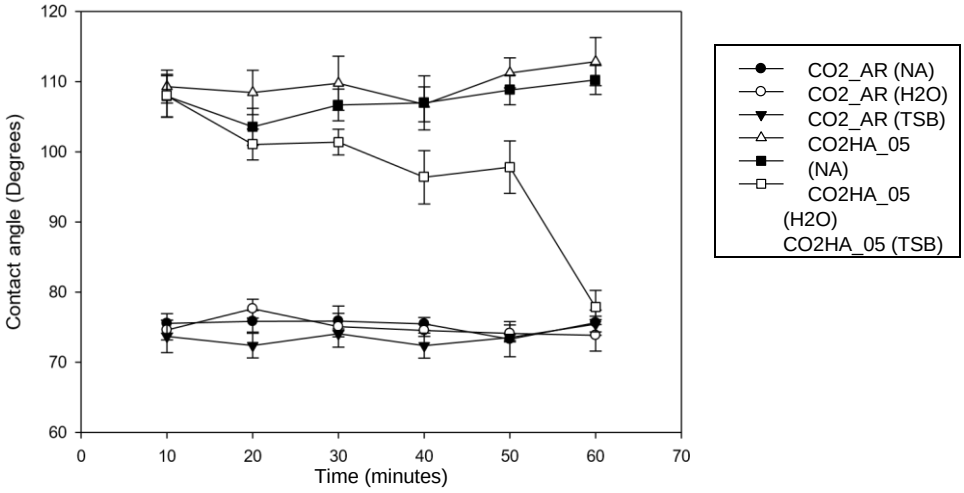


(b)

FIGURE 9

Comparison contact angle measurements of (a) CO2HA_04 with CO2_AR and (b) CO2HA_05 with CO2_AR.

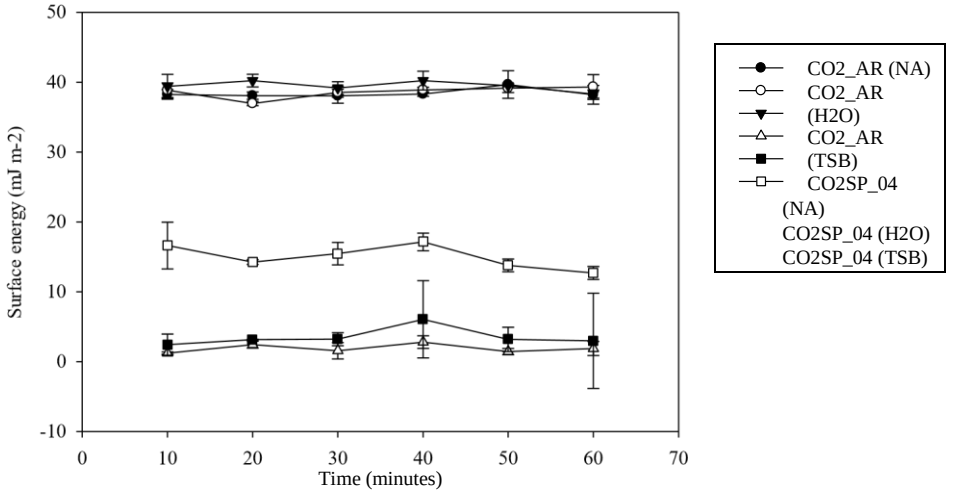


(a)

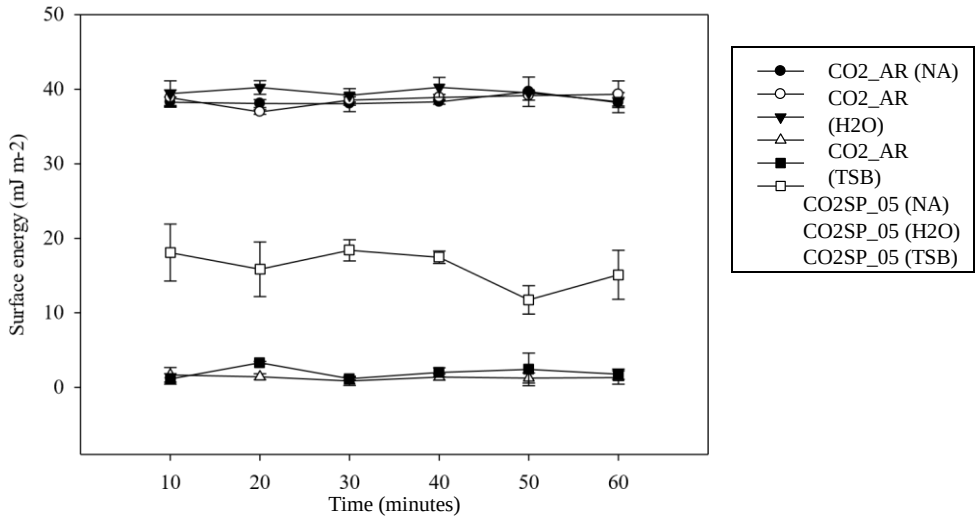


(b)

FIGURE 10

Comparison surface energy calculations of (a) CO2SP_04 with CO2_AR and (b) CO2SP_05 with CO2_AR.

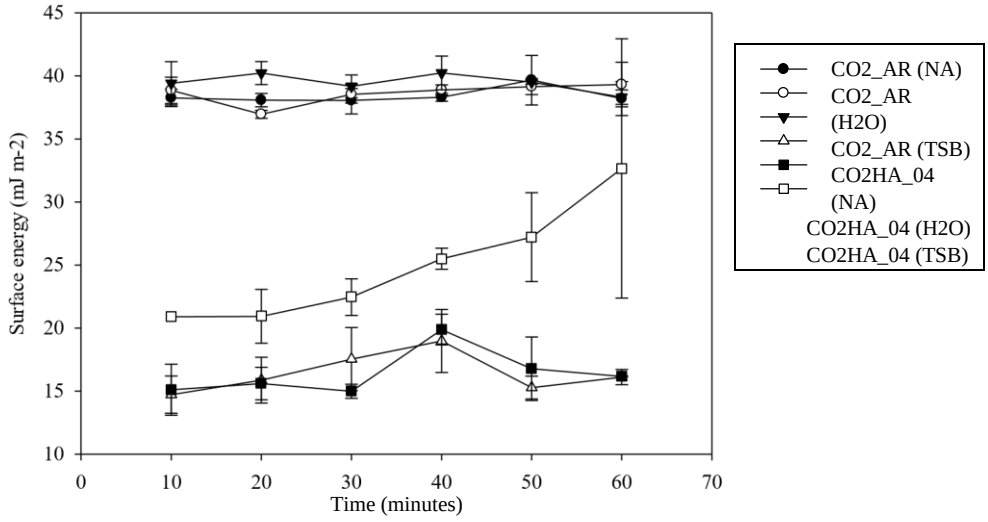


(a)

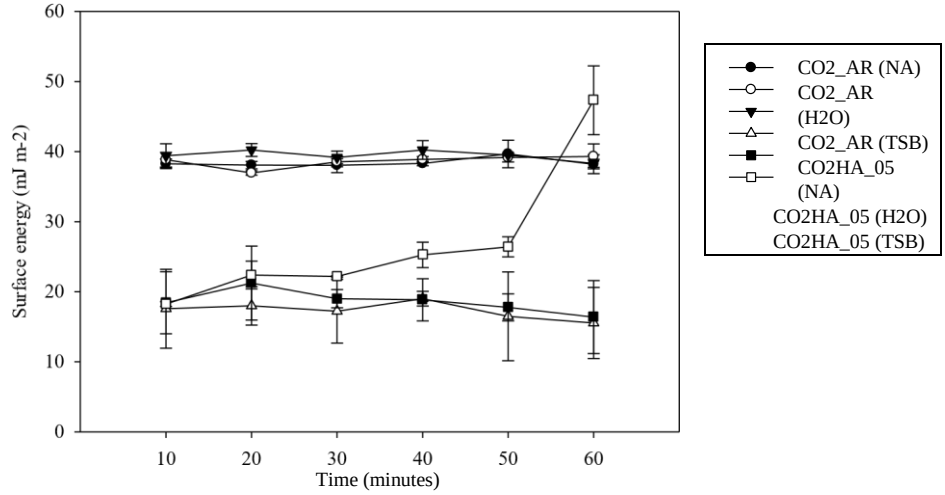


(b)

FIGURE 11

Comparison surface energy calculations of (a) CO2HA_04 with CO2_AR and (b) CO2HA_05 with CO2_AR.

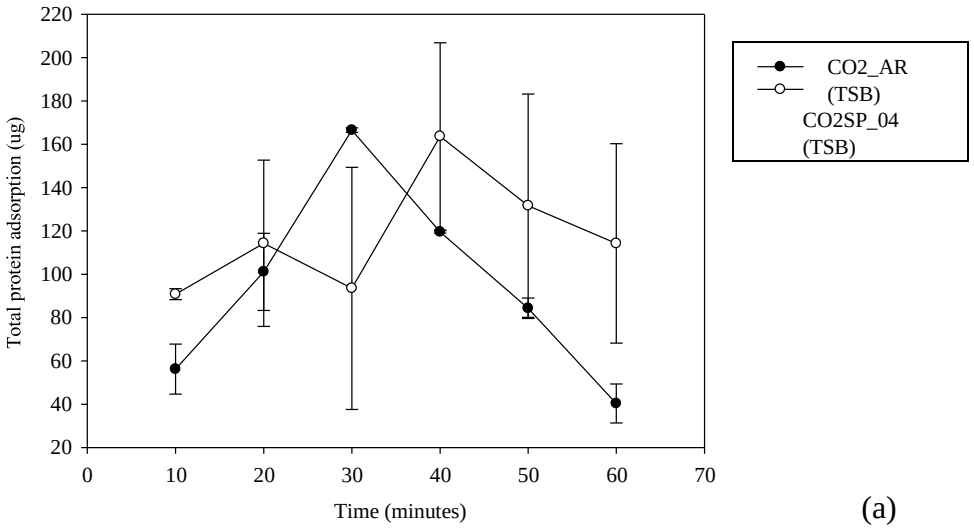
Total protein adsorption (ug)
Time (minutes)
CO2_AR (TSB)
CO2SP_04 (TSB)

(a)

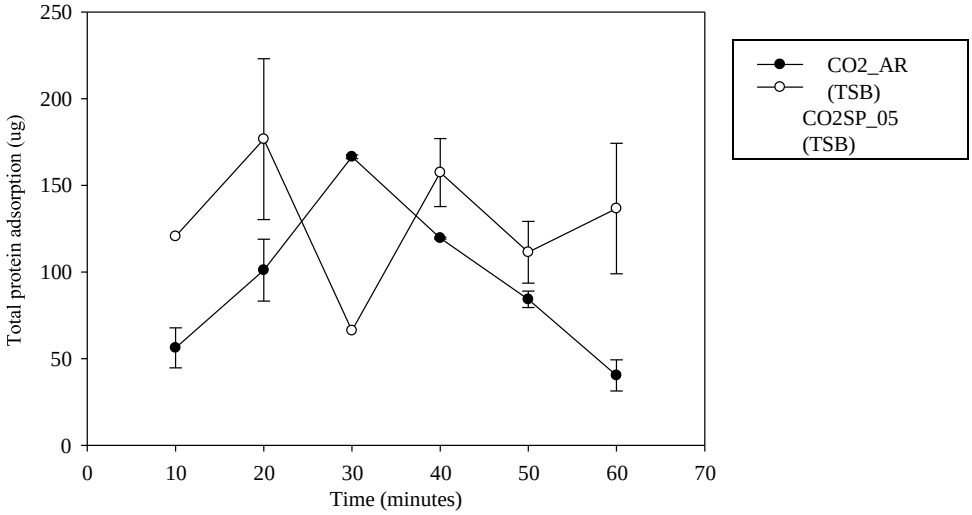
Total protein adsorption (ug)
Time (minutes)
CO2_AR (TSB)
CO2SP_05 (TSB)

(b)

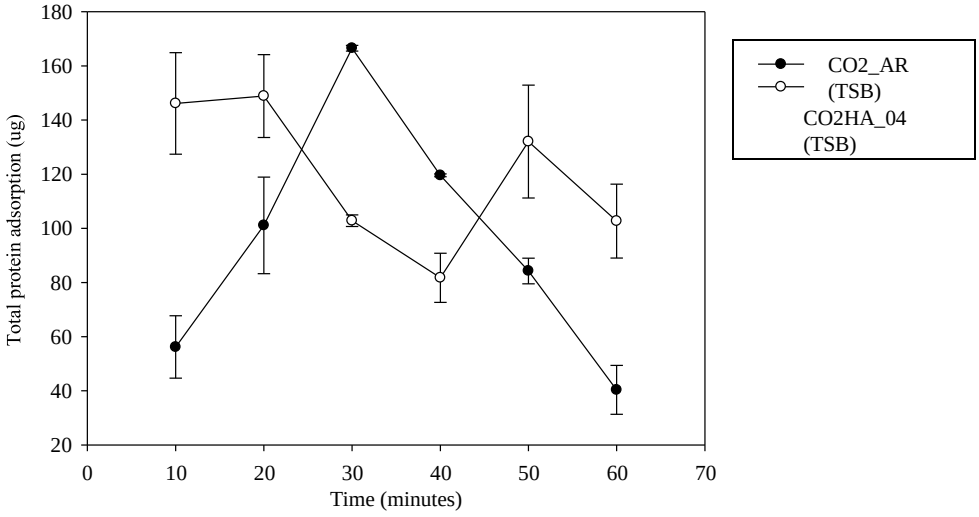
Total protein adsorption (ug)
Time (minutes)
CO2_AR (TSB)
CO2HA_04 (TSB)

(c)

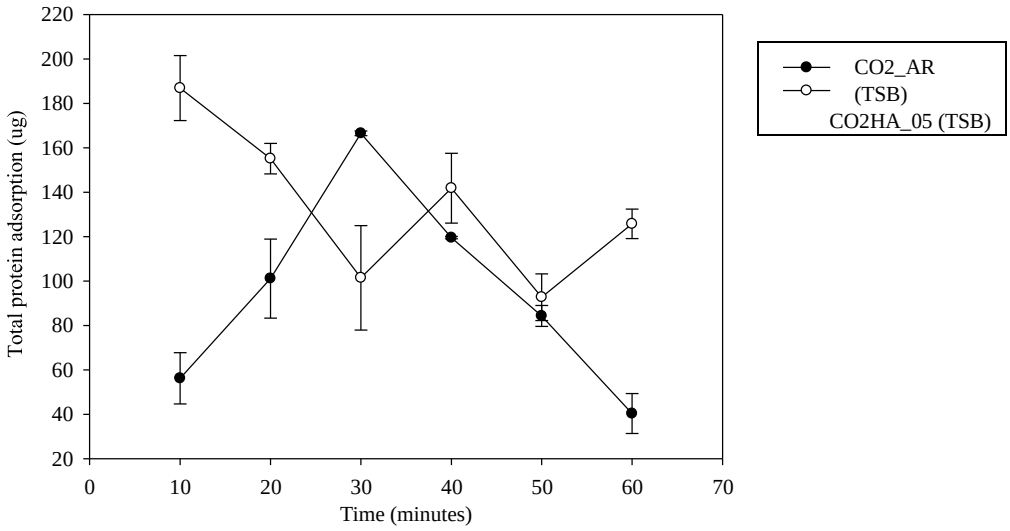


(d)

FIGURE 12

Variation in protein and biomolecule adsorption with incubation time for (a) CO2SP_04 compared to CO2_AR, (b) CO2SP_05 compared to CO2_AR, (c) CO2HA_04 compared to CO2_AR and (d) CO2HA_05 compared to CO2_AR.